Mechanosensitive kinetic preference of actin-binding protein to actin filament

Yasuhiro Inoue and Taiji Adachi

Phys. Rev. E **93**, 042403 — Published 7 April 2016

DOI: 10.1103/PhysRevE.93.042403

Mechanosensitive kinetic preference of actin-binding protein to actin filament

Yasuhiro Inoue* and Taiji Adachi
Department of Biomechanics, Institute for Frontier Medical Sciences Kyoto University, 53 Shogoinkawahara-cho, Sakyo-ku, Kyoto 606-8507, Japan

The kinetic preference of actin-binding proteins to actin filaments is altered by external forces on the filament. Such an altered kinetic preference is largely responsible for remodeling the actin cytoskeletal structure in response to intracellular forces. During remodeling, actin-binding proteins and actin filaments interact under isothermal conditions, because the cells are homeostatic. In such a temperature homeostatic state, we can rigorously and thermodynamically link the chemical potential of actin-binding proteins to stresses on the actin filaments. From this relationship, we can construct a physical model that explains the force-dependent kinetic preference of actin-binding proteins to actin filaments. To confirm the model, we have analyzed the mechanosensitive alternation of the kinetic preference of Arp2/3 and cofilin to actin filaments. We show that this model captures the qualitative responses of these actin-binding proteins to the forces, as observed experimentally. Moreover, our theoretical results demonstrate that depending on the structural parameters of the binding region, actin-binding proteins can show different kinetic responses even to the same mechanical signal *tension*, in which the double-helix nature of the actin filament also plays a critical role in a stretch-twist coupling of the filament.

Subject Areas: Biological Physics, Statistical Physics

I. INTRODUCTION

Actin is a ubiquitous, multiple-role protein in eukaryotic cells [1–3]. The assemblage of actin molecules into the actin cytoskeleton is mediated by actin-binding proteins (ABPs) [4–6]. Some ABPs bind to or dissociate from actin filaments (F-actin) in a mechanosensitive manner. Force spectroscopy using optical tweezers indicates that a non-covalent bond between F-actin and myosin II behaves as a catch bond, whose lifetime increases when stretched by mechanical forces [7]. Other studies have shown that tension in F-actin prevents cofilin binding prior to severing the F-actin [8], and that myosin II is recruited to stretched F-actin on the cell cortex [9]. F-actin branch formations induced by Arp2/3 binding can be biased by the curvature of the mother filament [10]. Thus, the mechanosensitive kinetics of ABPs on F-actin are no longer disputed. However, the mechanisms of the mechanosensitive kinetics of ABP–actin binding remain poorly understood. Elucidating these mechanisms is important for understanding how the actin cytoskeletal structure is modified by intracellular forces. To elucidate the mechanism of mechanosensitive kinetics, researchers have focused on the catch-bond behavior in dissociation pathways of the ligand–receptor bond (the so called catch-bond model) [11, 12]. The catch-bond model, which is an extension of Kramers' reaction–rate theory, successfully explains how the pulling ligand prolongs the bond lifetime, as observed under single-molecule force spectroscopy [7, 12]. However, the catch-bond model is limited to dissociation kinetics in the presence of a pulling ligand and cannot reveal how the kinetic preference of ABPs to F-actin changes under mechanical forces on the F-actin. Thus, we present a physical model that describes this mechanosensitive alternation of kinetic preferences. Using this model, we predict the number of ABPs bound to F-actin under given mechanical conditions.

* inoue@frontier.kyoto-u.ac.jp

II. KINETIC PREFERENCE EXPRESSED BY CHEMICAL POTENTIAL

The number of ABPs bound to F-actin can be determined by kinetically balancing the binding and unbinding processes between ABPs and F-actin. The balance is represented by an equilibrium constant. From a statistical mechanics perspective, the equilibrium constant quantifies the chemical potential difference between the bound and unbound states. The ABP–F-actin system is considered as a two-state system of bound and unbound states of the ABP–F-actin complex. State transitions can proceed from the unbound to the bound state or vice versa. The preferred direction of the transition depends on the chemical potential difference, $\Delta\mu$, between the bound and the unbound ABPs:

$$\Delta\mu = \mu^{\mathrm{b}} - \mu^{\mathrm{u}} \ , \tag{1}$$

where μ^{b} and μ^{u} denote the bound and unbound states, respectively.

The sign of $\Delta\mu$ determines the preferred state of the ABPs under the given mechanical conditions. For instance, positive (negative) $\Delta\mu$ indicates an increase in the number of unbound (bound) ABPs (Fig. 1). Our physical model expresses the change in the chemical potential difference, $\Delta\mu$, under an altered mechanical condition.

Two assumptions are imposed in the model. The kinetic assumption dictates that the chemical potential of the unbound state, μ^{u}, is unchanged throughout the

binding process. This implies that the number of unbound proteins in the cytosol is sufficiently large and remains essentially constant, despite the dynamic exchange of bound and unbound proteins.

The mechanics assumption describes the F-actin as a continuous elastic cylinder for estimating the deformation energy (Fig. 2A). This implies that the atomic-level energy changes of F-actin correlate well with the continuum-level energy changes. We focus on the linear elastic regime, wherein the F-actin deformation is the sum of the axial, bending, and torsional deformations. We consider an axial force exerted along the actin filament and conduct analogous analyses on the bending and torsional moments of the filament.

The axial forces induce the elastic stress σ within the ABP–actin complex. A stress change $\mathrm{d}\sigma$ alters the chemical potential $\mathrm{d}\mu^{\mathrm{b}}$ of the bound ABPs. This relationship, given by the Gibbs–Duhem equation [13], constrains the intensive parameters in the thermodynamic system. Under isothermal conditions, the chemical potential change satisfies

$$v\mathrm{d}\sigma + \mathrm{d}\mu^{\mathrm{b}} = 0 \ , \tag{2}$$

where v is the volume of the binding region of the ABP–actin complex within the actin filament. Equation (2) means that the intensive variables (stress and chemical potentials) cannot change independently.

To fully express the chemical potential μ^{b}, we note that the linear elastic deformation of the actin filament obeys Hooke's law:

$$\sigma = E\epsilon \ , \tag{3}$$

where E and ϵ are the Young's modulus and axial strain of the ABP–actin complex filament, respectively.

Integrating Eq. (2), we obtain

$$\mu^{\mathrm{b}}(\epsilon) = \mu^{\mathrm{b}}(\epsilon_{\mathrm{i}}) - \frac{v_0 E}{2}\left(\epsilon - \epsilon_{\mathrm{i}}\right)\left(\epsilon + \epsilon_{\mathrm{i}} + 2\right), \tag{4}$$

where $\mu^{\mathrm{b}}(\epsilon_{\mathrm{i}})$ is the chemical potential under the inherent strain ϵ_{i} induced by the binding of an ABP to a free filament, and v_0 is the volume of the binding region in the stress–free state (Fig. 2B). According to Eq. (4), the strain ϵ decreases the chemical potential. The chemical potential difference, $\Delta\mu(\epsilon)$, is directly obtained by subtracting μ^{u} from $\mu^{\mathrm{b}}(\epsilon)$.

We now model the case of moments exerted on the actin filament. A bending moment on the actin filament induces a surface strain ϵ, which is a function of the diameter d and curvature, c, of the filament:

$$\epsilon = -\frac{cd}{2} \ . \tag{5}$$

Here, positive curvature denotes that the normal vector of the curvature is *interior looking* (Fig. 2C). By substituting Eq. (5) into Eq. (4), the chemical potential of ABPs on a bent actin filament becomes a function of the curvature c:

$$\mu^{\mathrm{b}}(c) = \mu^{\mathrm{b}}(c_{\mathrm{i}}) - \frac{v_0 E d}{8}\left(c - c_{\mathrm{i}}\right)\left(cd + c_{\mathrm{i}}d - 4\right) \ , \tag{6}$$

where $c_{\mathrm{i}} = -2\epsilon_{\mathrm{i}}/d$ is the inherent curvature.

Finally, we model the case of torque T_θ exerted on the actin filament. The corresponding Gibbs-Duhem equation under the isothermal condition is given by

$$\theta\mathrm{d}T_\theta + \mathrm{d}\mu^{\mathrm{b}} = 0 \ . \tag{7}$$

To fully express μ^{b}, we again assume a linear elastic torsional deformation of the actin filament:

$$T_\theta = \frac{\kappa\theta}{\delta_0} \tag{8}$$

where the torsional angle θ is defined along the axial length δ_0 of the binding region, and κ denotes the torsional rigidity (Fig. 2D). Integrating Eq. (7), we obtain

$$\mu^{\mathrm{b}}(\theta) = \mu^{\mathrm{b}}(\theta_{\mathrm{i}}) - \frac{\kappa}{2\delta_0}\left(\theta^2 - \theta_{\mathrm{i}}^2\right) \tag{9}$$

where $\mu^{\mathrm{b}}(\theta_{\mathrm{i}})$ is the chemical potential at an inherent torsional angle θ_{i}, induced by an ABP binding to a free filament.

III. BRANCH FORMATION INDUCED BY THE ARP2/3 COMPLEX PREFERENTIALLY FROM THE EXTENSIONAL STRAIN OF THE ACTIN FILAMENT

Preferential branch formation by the Arp2/3 on the convex face of a curved actin filament has been observed *in vitro* [10]. In this study, the relative branch density was quantified by the probability density ratio of the curvatures at the branch point to the curvature of the mother filament. The relative branch density monotonically increased with negative curvature, indicating that the extensional side of the Arp2/3-binding site of F-actin promotes either the binding of the Arp2/3 complex to F-actin, and/or the activation of bound Arp2/3 complex. The activation of the bound Arp2/3 complex is enhanced by nucleation promoting factors (NPFs) [14–16], while neither NPFs nor binding to the side of F-actin are necessary for the Arp2/3 complex to achieve the active conformation [17]. The extent of NPF stimulation is also not affected by the F-actin surface that the Arp2/3 complex binds to [15]. Therefore, we focus on the former possibility that the extensional side of F-actin promotes the binding of the Arp2/3 complex to F-actin.

To explain this mechanosensitive branch formation by Arp2/3 binding to the bent filament, our model calculates the chemical potential difference between the bound and unbound states of the Arp2/3-NPF-F-actin complex [15]. We consider a major chemical pathway in the branch nucleation [14, 15], and define the chemical potential difference between the bound and unbound states between the Arp2/3-NPF complex and F-actin (see Appendix A). Here, in the experiment [10], as F-actin was immobilized on a surface before incubation of branch nucleation, we neglected a possibility that the curvatures were promoted by branch formations. In terms of the

chemical potential, the relative branch density $\tilde{P}(c)$ is given by

$$\tilde{P}(c) = \frac{1}{\Pi} \exp\left[-\beta \Delta\mu(c)\right], \tag{10}$$

where

$$\Pi = \int \exp\left[-\beta \Delta\mu(c)\right] P_{\mathrm{mf}}(c) \mathrm{d}c. \tag{11}$$

Here, $P_{\mathrm{mf}}(c)$ is the probability density of the mother filament curvature, and the thermal energy is defined as $\beta^{-1} = \mathrm{k_B}T$. Equation (10) is derived in the Appendix A.

According to the experimental data [10], the relative branch density is the unity at zero curvature. Therefore, the constant Π is computed as

$$\Pi = \exp\left[\beta \Delta\mu(0)\right], \tag{12}$$

and Eq.(10) becomes

$$\tilde{P}(c) = \exp\left[-\beta(\mu^{\mathrm{b}}(c) - \mu^{\mathrm{b}}(0))\right], \tag{13}$$

where we assume that the unbound-Arp2/3-NPF chemical potential μ^{u} is constant and independent of the F-actin curvature. Most of model parameters were obtained from experimental data of other studies (see Table I). The only unknown parameter was the binding region volume v_0. To predict this parameter, we minimized the least–squares of error between the model and experimental data. If the mathematical expression was incorrect, our model could not replicate the qualitative phenomena even after fitting all parameters.

Our model qualitatively captures the dependence of the relative branch density on the mother filament curvature (Fig. 3); namely, the increased density at negative curvatures. Thus, the mathematical expression of the model adequately explains the mechanosensitive branch formation. Moreover, it provides novel microscopic insight into the preferential branch formation. The maximum and minimum chemical potentials over the modeled range differ by nearly $\mathrm{k_B}T$, comparable to the energy of one salt bridge between two amino acids [18]. Therefore, the net breakage or net additional formation of one salt bridge may rectify curvature-biased branch formation. Because the model assumes that the axial strain modifies the chemical potential energy to satisfy the Gibbs–Duhem equation, we speculate that the unbound state can be converted to the bound state merely by stretching the filament; bending may not be necessary.

A shift in the average curvature of the filament breaks the symmetry of the bending fluctuation with respect to the curvature sign. Preferential branch formations under such asymmetric conditions have been investigated by the fluctuation gating (FG) model [10]. The FG model imposes a threshold curvature c_{th} beyond which the Arp2/3 stably binds and initiates branching. The asymmetry of the fluctuating curvature can bias the probabilities of stable binding and branching. Thus, the FG model also captures the qualitative dependence of the relative branch density on the filament curvature. However, our proposed and the FG models would differently predict the branch formations on a tensile filament. The FG model predicts that a branch formation cannot be promoted or strongly suppressed because the axial tensile force reduces the bending fluctuation of the filament [19]. In contrast, our model predicts that an extensional strain on the tensile filament will trigger branch formation where, by substituting the predicted value of v_0 into Eq. (4), we estimate that the tensile force of 100 pN on F-actin increases the equilibrium constant K_{e} by 24% when compared with that of the stress free state. Thus, both models require validation by the experimental observations of Arp2/3–induced branch formation on tensile filaments. Such observations present an exciting experimental challenge.

IV. COFILIN-ACTIN BINDING SUPPRESSED BY UNTWISTING ACTIN FILAMENT

When actin filaments are decorated by cofilin molecules, they are additionally twisted by 5° per 2.75 nm [20], suggesting that changing the pitch of the helical actin filament affects the cofilin–actin binding. In fact, tension in the actin filament prevents cofilin from binding to the filament [8]. Moreover, on account of the double helical nature of actin filaments, the tension generates a torsional moment on the filament through stretch–twist coupling [21, 22]. Using our model, we investigate how changes in the axial strain and pitch of the actin helix upon cofilin-actin binding alter the chemical potential difference.

We consider both the binding and unbinding of cofilin on the filament. At chemical equilibrium, the relative cofilin–bound density $\tilde{P}(\epsilon, \theta)$ defined in the previous section:

$$\tilde{P}(\epsilon, \theta) = \frac{1}{\Pi} \exp[-\beta \Delta\mu(\epsilon, \theta)], \tag{14}$$

where

$$\Pi = \int\int \exp[-\beta \Delta\mu(\epsilon, \theta)] P_{\mathrm{mf}}(\epsilon, \theta) \mathrm{d}\epsilon \mathrm{d}\theta, \tag{15}$$

$$\Delta\mu(\epsilon, \theta) = \Delta\mu(\epsilon) + \Delta\mu(\theta). \tag{16}$$

Here, $P_{\mathrm{mf}}(\epsilon, \theta)$ denotes the probability density under axial strain ϵ at the torsional angle θ of the mother filament.

Because the binding region volume v_0 is unknown, we predict how the chemical potential difference responds to the axial strain and helical pitch in three regimes: (A) $v_0 E \ll \kappa/\delta_0$, (B) $v_0 E \sim \kappa/\delta_0$, and (C) $v_0 E \gg \kappa/\delta_0$, where $v_0 E$ and κ/δ are competing energy terms. To analyze the effect of axial strain and helical pitch on the chemical potential difference, we present the contour plots of the change in chemical potential difference, defined as $\mathrm{d}\Delta\mu(\epsilon, \theta) = \Delta\mu(\epsilon, \theta) - \Delta\mu(\epsilon_{\mathrm{i}}, \theta_{\mathrm{i}})$ (see Fig. 4). Because a tensile force increases the axial strain on the filament and untwists the helical pitch [22], the chemical potential difference changes along the helical pitch

axis (from right to left) and along the strain axis (from bottom to up) in Fig. 4.

More specifically, the chemical potential difference increases as the helical pitch untwists and decreases as the axial strain increases. To explain the tension–induced suppression of cofilin–actin binding, the chemical potential difference should increase under tensile force. Therefore, the axial strain should contribute much less to the chemical potential difference than the untwisting of the helical pitch, implying that $v_0 E \leq \kappa/\delta_0$ (panel A and B of Fig. 4). Hereafter, we neglect the axial strain contribution and discuss the relative cofilin-bound density as the torsional fluctuation reduces under tension.

The severing of the actin filaments by cofilin is prevented or delayed by very small forces (several piconewtons) [8]. Because a tensile force of several piconewtons will scarcely change the helical pitch, we question whether a slight untwisting of the helix in our model can replicate the tension-induced suppression of cofilin–actin binding. Experimentally, a 5–pN tensile force reduces the torsional fluctuation by approximately 60% [8], indicating that the torsional rigidity was approximately 2.5 times higher under tension than in the tension–free state. Therefore, we investigated the effect of torsional rigidity on the relative cofilin-bound density $\tilde{P}(\theta)$. The results are plotted in Fig. 5, where the relative density is normalized by its value at the inherent helix pitch.

According to this figure, the untwisting of the helical pitch induces a steeper change in $\tilde{P}(\theta)$ under higher torsional rigidity (tension) than under lower torsional rigidity (tension–free). In the tense state, untwisting of the helix by 0.7 (deg/2.75 nm) nearly halves the relative cofilin-bound density; in the relaxed state, an untwisting of approximately 2.6 (deg/2.75 nm) is required to halve the relative cofilin–bound density. Thus, our theoretical model suggests that high torsional rigidity (equivalently, low torsional fluctuation) plays a pivotal role in suppressing cofilin–actin binding.

Because cofilin binding increases fluctuation of F-actin [23], and because a positive correlation between cofilin binding and fluctuation of F-actin was presented using single–molecule imaging analysis [24], we further focus on the relationship between cofilin bindings and the fluctuation of F-actin. Based on Eq. (9), we obtain a mathematical equation expressing how the on–rate of cofilin binding to the actin filament is altered by the torsional fluctuation as follows.

$$\frac{k_{\mathrm{on}}}{k_{\mathrm{on}}^{(\mathrm{r})}} = \sqrt{\frac{\langle\theta_{\mathrm{r}}^2\rangle}{\langle\theta^2\rangle}} \exp\left(-\beta\frac{\kappa_{\mathrm{r}}\theta_{\mathrm{i}}^2}{2\delta_0}\left(\frac{\langle\theta_{\mathrm{r}}^2\rangle}{\langle\theta^2\rangle}-1\right)\right) \qquad (17)$$

Here, $\langle\theta^2\rangle$ is the variance of the torsional angle, k_{on} is the on–rate of cofilin binding, and super- and subscript r indicate values at an arbitrary reference state r. We give a derivation of Eq (17) in the Appendix B. In the derivation, we find that the on-rate of cofilin depends on the torsional fluctuation of F-actin, unless the chemical potential difference is independent of the torsional angle. Therefore, the dependence of the on-rate on torsional fluctuation is expected to show evidence for a dependence of the chemical potential difference on the torsional angle.

Figure 6 shows good agreement between the experimental result and our model prediction, where we do not fit parameters in Eq. (17) to the data, but just employ values measured experimentally in previous studies [23–25]. Because cofilin would access F-actin at its favored torsional angle θ_{i} by chance, a decrease of torsional fluctuation of F-actin results in a decrease of probability that cofilin is able to access F-actin at θ_{i}, leading to a decrease of the on-rate.

Here, because Hayakawa et al. analyzed the single-molecule imaging data in terms of their originally defined parameter, index of fluctuation (IF), instead of torsional fluctuation [24], we explain how we plot Fig. 6 as follows. At first, because IF was calculated based on the standard deviation of the fluorescence intensity of each pixel along the filament [24], IF represent mixtures of longitudinal, bending and torsional fluctuations of F-actin, where the pixel size was 85 nm, which is approximately double spacing of a crossover of the filament helix. At this pixel scale, torsional fluctuation contributes primarily to IF rather than longitudinal and bending fluctuations, implying IF $\propto \sqrt{\langle\theta^2\rangle}$. This is because Young's modulus is very high and the persistence length of the actin and cofilactin filaments are approximately 10 μm and 2 μm, respectively [23], indicating that F-actin is straight and unchanged at the length of the pixel scale. Then, we normalized the magnitude of the index of fluctuation by IF = 4.5 as the reference state, namely, $\sqrt{\langle\theta^2\rangle\,/\,\langle\theta_{\mathrm{r}}^2\rangle} = \mathrm{IF}/4.5$. This is because the on–rate at the reference state (IF = 4.5) is 0.08, which is almost the same as the mean value of the on–rate measured in [24]. Thus, we could essentially adopt the value of torsional rigidity without requiring the external force measured in [23, 25] as the value of κ_{r}.

V. DISCUSSION

We proposed a physical model based on the Gibbs–Duhem equation. Our model explains how mechanical forces alter the kinetic preference of ABPs to F-actin. Moreover, the model captures the qualitative dependence of the relative branch density on the mother filament curvature, as experimentally observed in Arp2/3–induced actin branching. Our model also suggests that Arp2/3–actin binding can be promoted by stretching an actin filament. Following the successful theoretical demonstration of curvature-biased branching, we applied the model to the suppression of cofilin binding by tense actin. We found that the tension–induced untwisting of the F-actin helix sufficiently suppresses cofilin–actin binding. Then, based on the model, we have obtained the theoretical relationship between the on-rate of cofilin binding and the torsional fluctuation of F-actin. The theoretical relationship was confirmed by the corresponding experimental data without fitting any model parameters, showing good

agreement between the model and its corresponding experiment. The reduced torsional fluctuation is essential for suppressing the binding of cofilin.

We suggest that, depending on the ABPs, the ABP–actin system might respond differently (i.e., might promote or suppress binding) to the same mechanical signal *tension*. The double–helix nature of F-actin plays a critical role in these complementary responses because it allows the conversions of the mechanical signal *tension* to another mechanical signal, *torsion*. These two mechanical deformations of F-actin (stretch and torsion) can be recognized by various ABPs. Because the mechanical deformation that mainly changes the chemical potential difference depends on the volume v_0 and the axial length δ_0 of the binding region, ABPs may be evolutionary adapted to certain values of v_0 and δ_0; for instance, $v_0 E \leq \kappa/\delta_0$ and $v_0 E \gg \kappa/\delta_0$ may suppress cofilin–actin binding and promote Arp2/3–actin binding, respectively. The latter might also promote actin–myosin II binding, as myosin II likely binds to stretched F-actin [9]. Therefore, to better understand the mechanosensitive ABP–actin kinetics from the molecular to kinetic levels, we must relate structural information on F-actin binding sites to physical information, quantified by v_0 and δ_0.

Our model represents the mechanical properties of F-actin by the constitutive equations of elasticity. Therefore, it can be rendered applicable to other molecular systems by selecting an alternative constitutive equation. In the presence of ATP, kinesin preferentially binds near other bound kinesin molecules at the plus-end of the microtubule [26]. If the binding probability were quantified as a function of distance between the two adjacent bound kinesins, our model might predict whether kinesin can recognize microtubule distortions induced by an adjacently bound kinesin.

Finally, to our knowledge, there are only a few experimental studies that describe quantitatively the mechanosensitive kinetic preference (except the catch-slip-bond behavior), and currently, all existing quantitative data can be described by mechanosensitivities of branching [10] and severing [24] of F-actin, which we could explain using our model. Lack of experimental data currently hampers interpretations of results describing the kinetics of ABPs together with the (microscopic) mechanical state of F-actin, such as strain, curvature and torsion. Because single-molecule imaging techniques are still growing rapidly, there could be opportunities for testing our model by possible future experiments that quantify either the on-rate or off-rate of ABPs with respect to the mechanical state of F-actin. There might also be unawareness of the emergence of mechanosensitive kinetics in mechanically stimulated F-actin. This is due to the lack of theoretical concepts. Namely, there is a body of experimental data describing the off-rate of ABPs (ligand) stimulated mechanically in which these are motivated by the theoretical concept of the catch-bond model (which expresses the off-rate of a stimulated ligand), while this is not the case of F-actin (receptor). We expect that our model offers another approach (besides catch-bond model) based on physics to understand mechanosensitive kinetics.

ACKNOWLEDGMENTS

A part of this research was supported by CREST, Japan Science and Technology Agency (JST), KAKENHI(25702025) from the Ministry of Education, Culture, Sports, Science and Technology (MEXT), Japan, and the Platform Project for Supporting in Drug Discovery and Life Science ResearchiPlatform for Dynamic Approaches to Living Systemjfrom the Japan Agency for Medical Research and development(AMED). Y. I. would like to thank Ms. Ayu Narita for her assistance in drawing the graphic of F-actin and Dr. Katsuhiko Sato (Hokkaido Univ) for valuable discussions.

TABLE I. Parameters

Symbol	Value	Unit	Description	Ref.
T	300	K	Temperature	[10]
E	1.8×10^{9}	Pa	Young's modulus of actin filament	[27]
d	5.6×10^{-9}	m	Diameter of actin filament	[27]
v_0	2.23×10^{-28}	m^3	Volume of Arp2/3-F-actin binding region	n/a[a]
κ	5×10^{-27}	Nm^2	Torsional rigidity of F-actin with tensile force	[8][b]
κ	2×10^{-27}	Nm^2	Torsional rigidity of F-actin without external force	[23, 25]
δ_0	3.7×10^{-9}	m	Axial length of the cofilin-F-actin binding region	[28][c]
ϵ_i	0.0	-	Inherent cofilin-F-actin strain	[20][d]
θ_i	1.17×10^{-1}	rad	Inherent cofilin-F-actin torsion angle in the length δ_0	[20]

[a] Predicted in this study
[b] Estimated from the torsional fluctuation
[c] Measured distance between α-carbons in residues K326 and K336 at the pointed and barbed subunits, respectively, based on the PDB file from Ref. [28].
[d] No significant difference in the axial rise per subunit between F-actin and cofilin–F-actin.

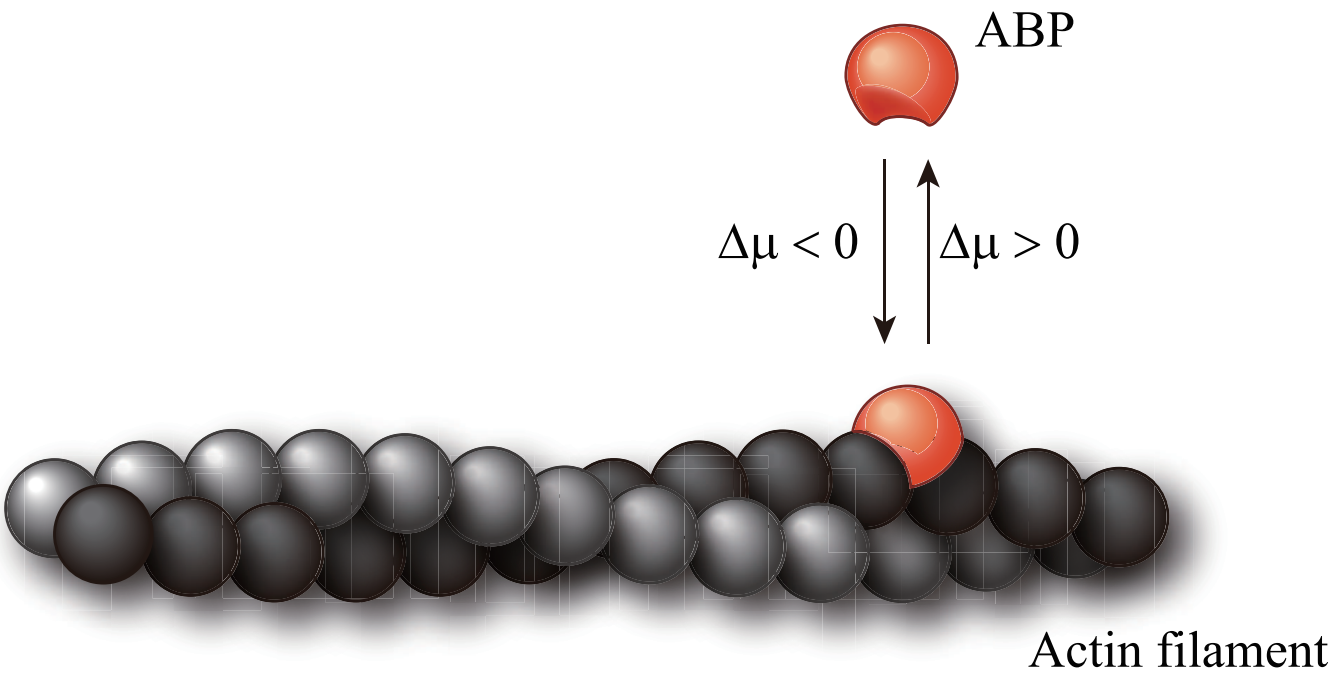

FIG. 1. Chemical potential difference, $\Delta\mu$, is defined by subtracting the chemical potential in the bound state from in the unbound state. Therefore, negative and positive $\Delta\mu$ denotes an increase in the number of bound and unbound ABPs, respectively.

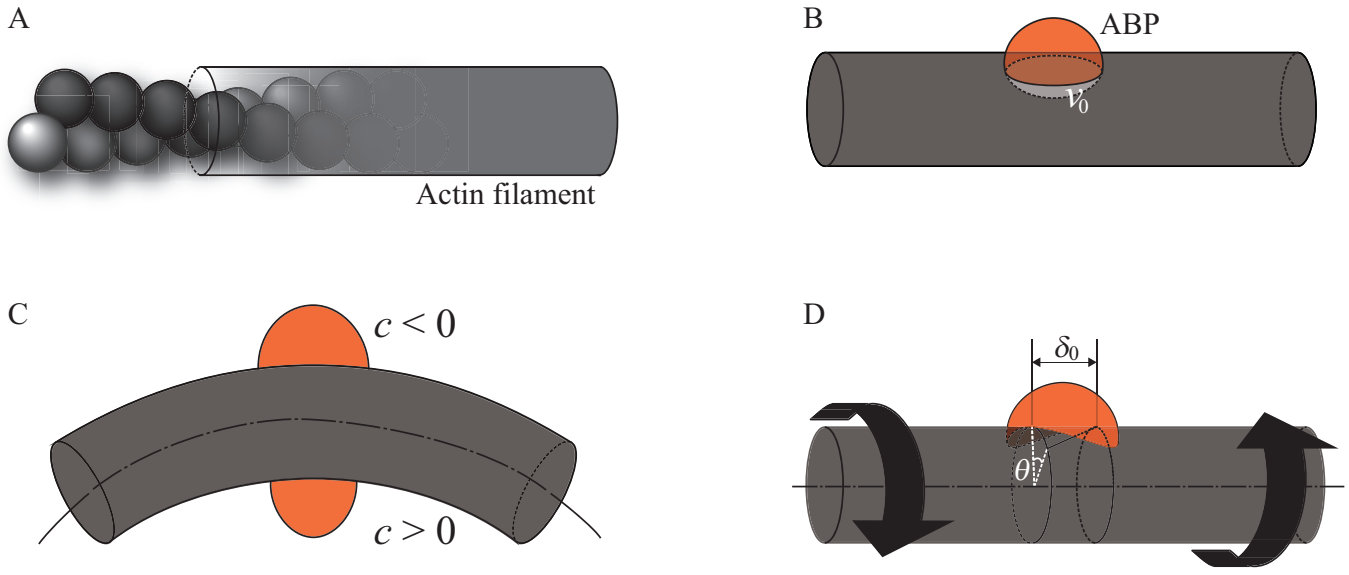

FIG. 2. Schematics of our model: (A) F-actin is modeled as a continuous elastic cylinder. (B) The volume v_0 of the binding region in the actin filament in the stress–free state. (C) Definition of the sign of the curvature c at two possible ABP-bound sides. (D) The torsional angle θ is defined along the axial length δ_0 of the binding region.

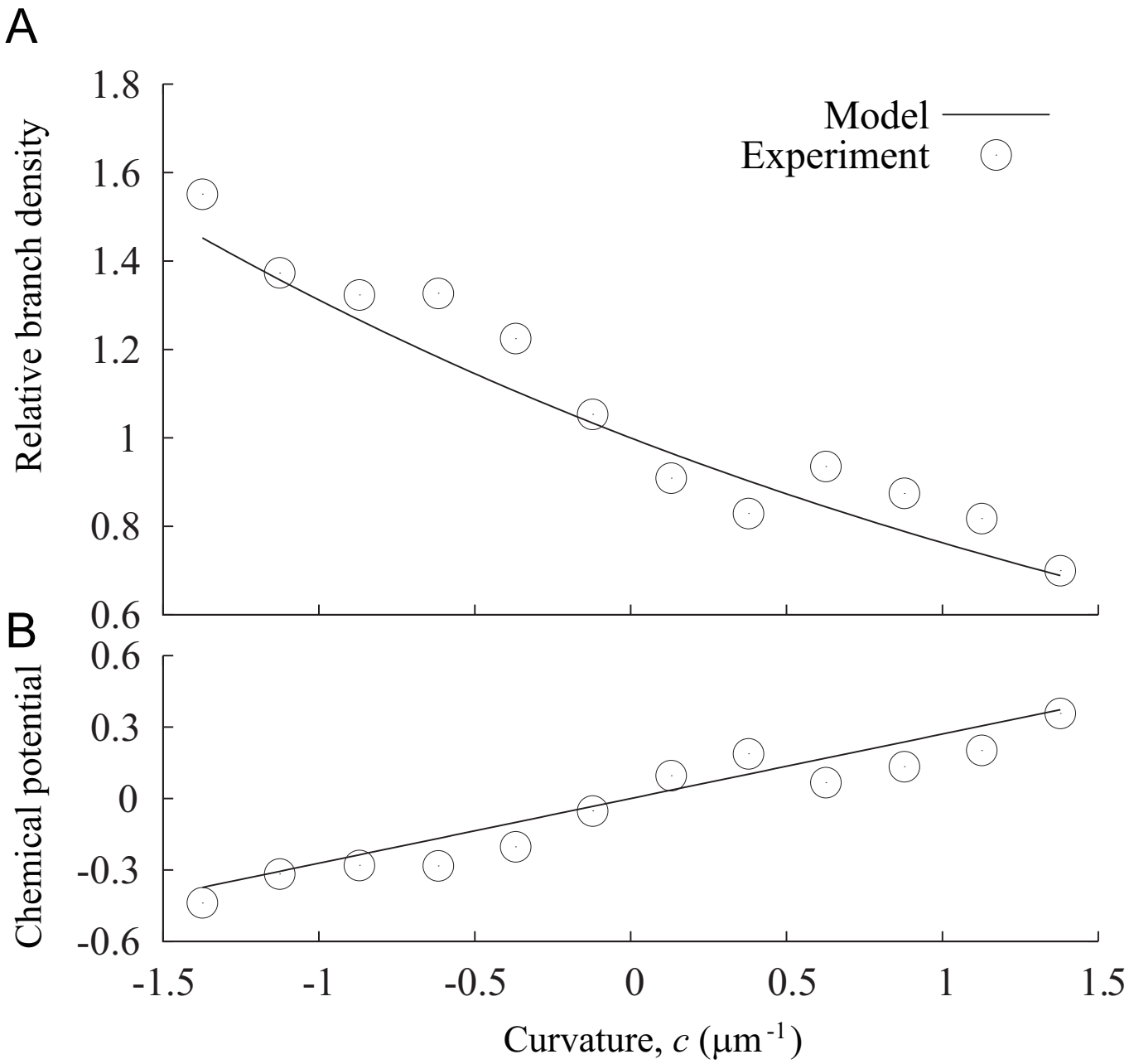

FIG. 3. (A) Relative branch density, $\tilde{P}(c)$, and (B) chemical potential $\mu^{\mathrm{b}}(c) - \mu^{\mathrm{b}}(0)$ (normalized by $k_{\mathrm{B}}T$) as functions of the mother filament curvature c: Circles and solid lines represent the experimental results of Risca et al. [10] and our model predictions Eq. (13), respectively.

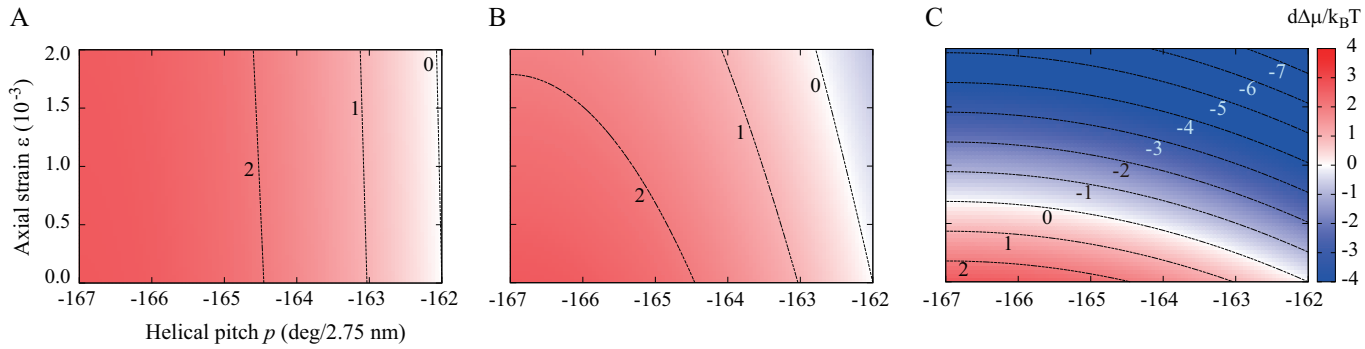

FIG. 4. Contour representations of the change in chemical potential difference, $d\Delta\mu$, of cofilin on tense and untwisted actin filaments, as functions of the axial strain ϵ and helical pitch p of the filament, where $p = -167 + 180(\theta/\pi)(2.75 \times 10^{-9}/\delta_0)$. The inherent axial strain and helical pitch of the cofilin-bound actin filament is 0 and -162 (deg/2.75 nm), respectively. $v_0 E =$ (A) $0.1\kappa/\delta_0$, (B) κ/δ_0, and (C) $10\kappa/\delta_0$.

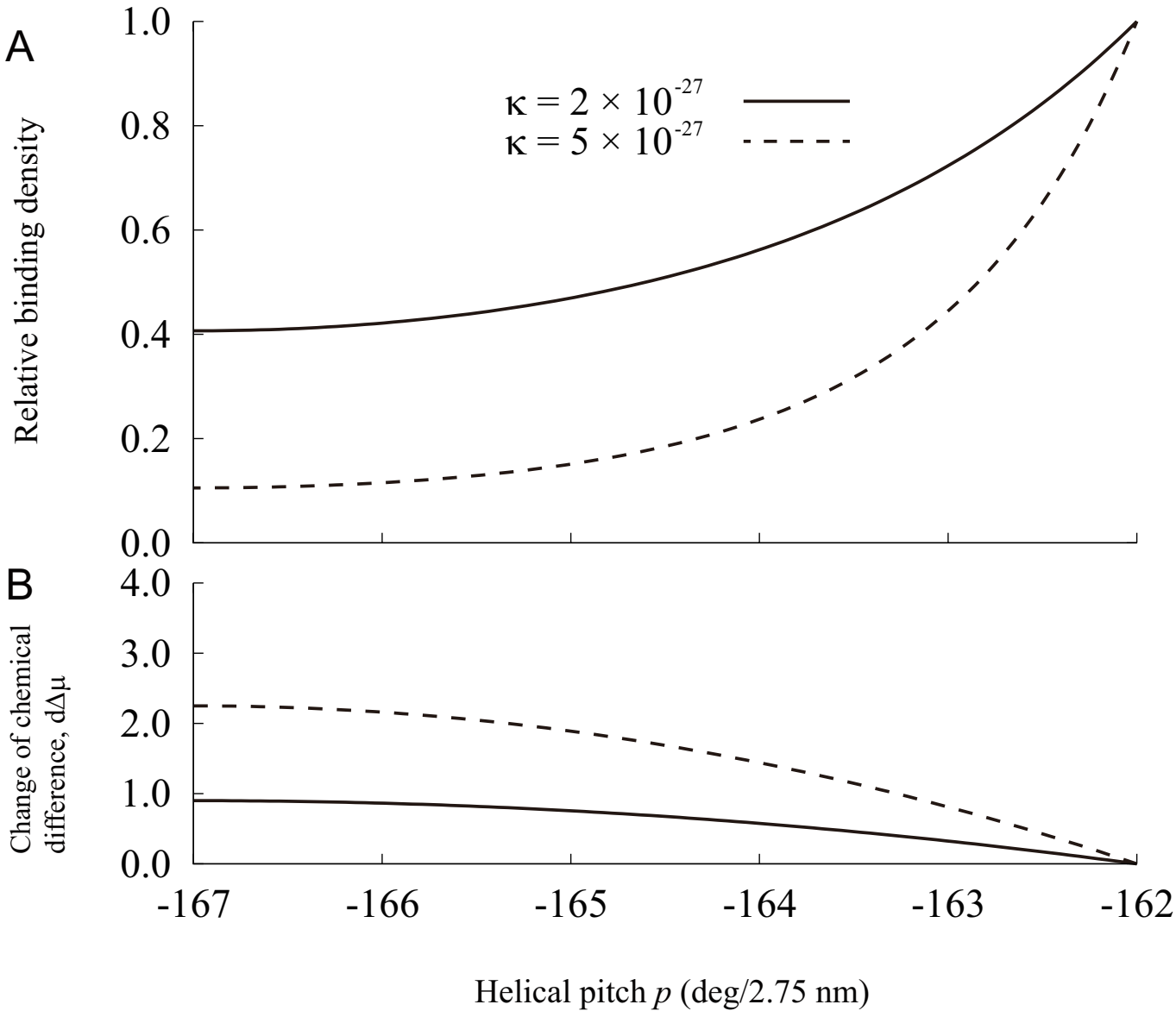

FIG. 5. Effect of torsional rigidity magnitude κ on (A) the relative cofilin-bound density, and (B) the change in the chemical difference (normalized by $k_{\mathrm{B}}T$). The horizontal axis indicates the pitch of the double helix of the actin filament, p, where $p = -167 + 180(\theta/\pi)(2.75 \times 10^{-9}/\delta_0)$. The inherent helical pitch of the cofilin-bound actin filament is -162 (deg/2.75 nm).

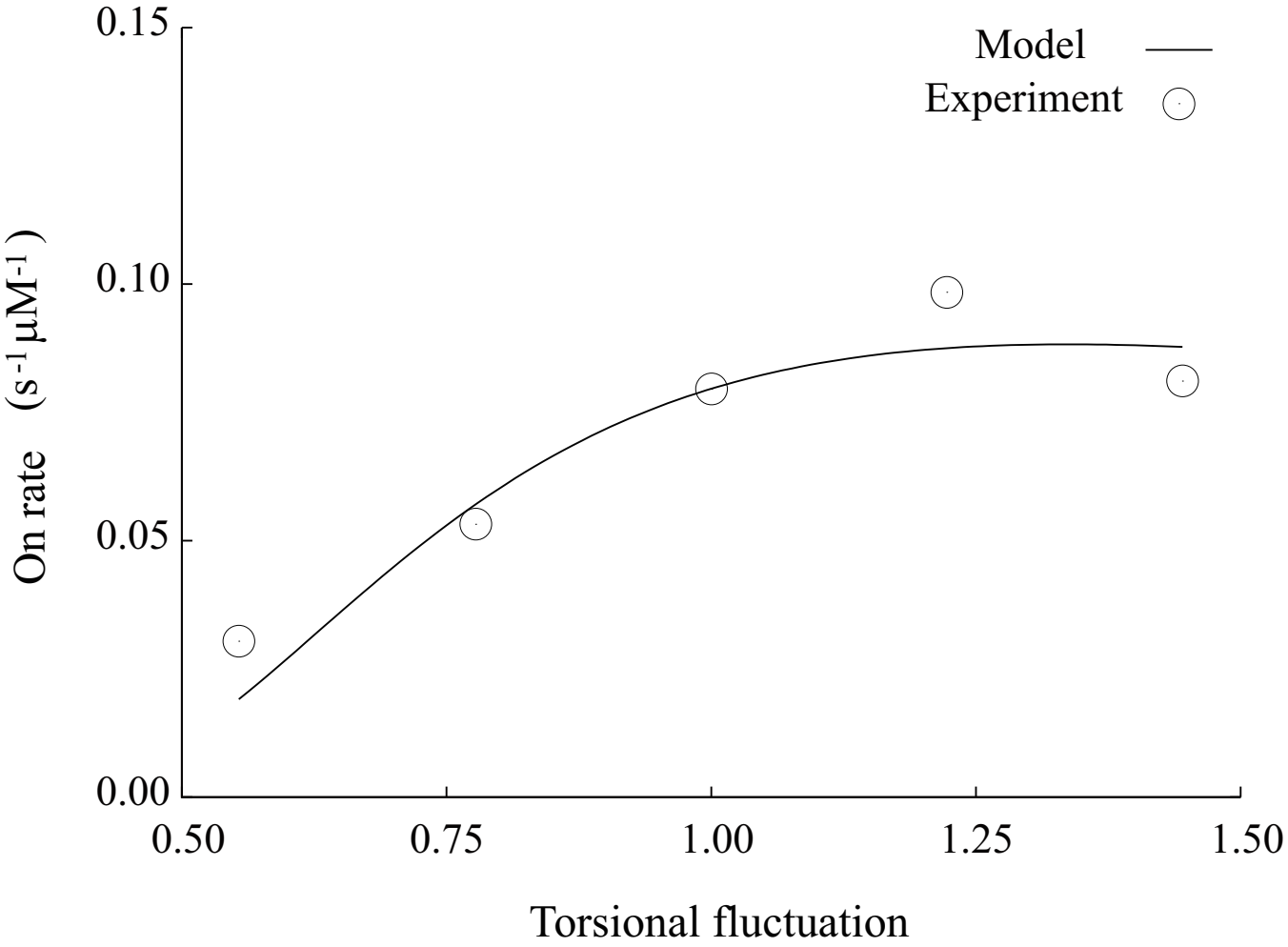

FIG. 6. Effect of torsional fluctuation on the on–rate of cofilin binding to the actin filament. Torsional fluctuation is normalized by that at the reference state r, $\sqrt{\langle\theta^2\rangle / \langle\theta_r^2\rangle}$. Circles and solid lines represent the experimental results of Hayakawa et al. [24] and our model predictions Eq. (17), respectively.

Appendix A: Reduced chemical pathway in branching formation

Arp2/3-induced branch formation proceeds in three steps: the Arp2/3 complex and nucleation promoting factor (NPF) bind to F-actin, branch nucleation is activated from the Arp2/3–NPF–F-actin complex, and the daughter filament elongates [14, 15]. Because the elongation step proceeds from the distal side of the bound Arp2/3–NPF complex away from its tethering site on F-actin, and because the extent of NPF stimulation is not affected by its tethering surface of F-actin [15], we speculate that the curvature of F-actin affects the binding steps predominantly. Although there are several possible pathways from Arp2/3, NPF and actins to branched F-actin, the major pathway is considered to be the following [14, 15]:

$$\text{Arp2/3-NPF} + \text{ABS} \underset{k_{\text{off}}}{\overset{k_{\text{on}}}{\rightleftharpoons}} \text{Arp2/3-NPF-ABS} \tag{A1}$$

$$\text{Arp2/3-NPF-ABS} \overset{k_{\text{ac}}}{\rightharpoonup} (\text{Arp2/3-NPF})^*\text{-ABS} \tag{A2}$$

Here, ABS indicates an Arp2/3 binding site on the F-actin surface. Activated bound states of the Arp2/3–NPF–F-actin complex are denoted by (Arp2/3–NPF)*–ABS. The corresponding kinetic equations are given by

$$\frac{\mathrm{d}}{\mathrm{d}t}[\text{Arp2/3-NPF-ABS}] = k_{\text{on}}[\text{Arp2/3-NPF}][\text{ABS}] - \mathrm{k}_{\text{off}}[\text{Arp2/3-NPF-ABS}] - \mathrm{k}_{\text{ac}}[\text{Arp2/3-NPF-ABS}] \ , \tag{A3}$$

$$\frac{\mathrm{d}}{\mathrm{d}t}[(\text{Arp2/3-NPF})^*\text{-ABS}] = k_{\text{ac}}[\text{Arp2/3-NPF-ABS}] \ . \tag{A4}$$

Square brackets $[\cdot]$ indicate the density of quantity $\cdot$. Because the efficiency of activating bound Arp2/3 is very low even at maximally activating concentrations of NPF and the off–rate is very high ($k_{\text{ac}}/k_{\text{off}} \ll 1$) [15], we can approximate Eq. (A3) as follows.

$$\begin{aligned}&\frac{\mathrm{d}}{\mathrm{d}t}[\text{Arp2/3-NPF-ABS}] \\ &\simeq k_{\text{on}}[\text{Arp2/3-NPF}][\text{ABS}] - \mathrm{k}_{\text{off}}[\text{Arp2/3-NPF-ABS}]\end{aligned} \tag{A5}$$

Thus, in the chemical equilibrium, a balance between binding and unbinding of Arp2/3-NPF and F-actin, and initial reactants and final products are related by

$$\begin{aligned}&[(\text{Arp2/3-NPF})^*\text{-ABS}]_{\text{eq}} \\ &= \lambda K_{\text{e}}[\text{Arp2/3-NPF}]_{\text{eq}}[\text{ABS}]_{\text{eq}} \ ,\end{aligned} \tag{A6}$$

$$\lambda = k_{\text{ac}}\tau \tag{A7}$$

$$K_{\text{e}} = \frac{k_{\text{on}}}{k_{\text{off}}} \ , \tag{A8}$$

where λ and K_{e} are the efficiency of branching activation and the equilibrium constant, respectively. τ is incubation time (*cf.* 70–120 s [10]). The chemical potential of this reduced process can be related to the equilibrium constant:

$$\Delta\mu = -\frac{1}{\beta}\ln K_{\text{e}} \ . \tag{A9}$$

In deriving the above relationship, we ignored the curvature of the mother filament. By the same approach, we now derive the corresponding chemical process on the filaments of curvature c, thereby rewriting the densities as

$$\rho_{\text{A}} := [\text{Arp2/3-NPF}] \ , \tag{A10}$$

$$\rho_{\text{F}}(c) := [\text{ABS}] \text{ at the curvature } c, \tag{A11}$$

$$\rho_{\text{FA}}(c) := [\text{Arp2/3-NPF-ABS}] \text{ at } c, \tag{A12}$$

$$\rho_{\text{FA}^*}(c) := [(\text{Arp2/3-NPF})^*\text{-ABS}] \text{ at } c, \tag{A13}$$

the kinetic equation of the reduced chemical process becomes

$$\frac{\mathrm{d}}{\mathrm{d}t}\rho_{\text{FA}}(c) = k_{\text{on}}(c)\rho_{\text{A}}\rho_{\text{F}}(c) - k_{\text{off}}(c)\rho_{\text{FA}}(c) \tag{A14}$$

$$\frac{\mathrm{d}}{\mathrm{d}t}\rho_{\text{FA}^*}(c) = k_{\text{ac}}\rho_{\text{FA}}(c) \tag{A15}$$

where the kinetic constants $k_{\text{on}}(c)$ and $k_{\text{off}}(c)$ also depend on the curvature c.

Considering that most of the binding sites are not occupied by Arp2/3 complexes, we approximate the density of free binding sites at curvature c by the total density of binding sites at the same curvature.

$$\rho_{\text{F}}(c) \simeq \rho_{\text{F}}^{\text{total}}(c) \tag{A16}$$

Then,

$$\frac{\mathrm{d}}{\mathrm{d}t}\rho_{\text{FA}}(c) \simeq k_{\text{on}}(c)\rho_{\text{A}}\rho_{\text{F}}^{\text{total}}(c) - k_{\text{off}}(c)\rho_{FA}(c) \tag{A17}$$

In chemical equilibria, the equilibrium density of reactants and product is given by

$$\rho_{\text{FA}^*}(c) = \lambda\exp(-\beta\Delta\mu(c))\rho_{\text{A}}\rho_{\text{F}}^{\text{total}}(c) \tag{A18}$$

here,

$$\Delta\mu(c) = -\frac{1}{\beta}\ln K_{\text{e}}(c) \ . \tag{A19}$$

The fraction $P(c)$ of branches at curvature c is then defined as

$$P(c) := \frac{\rho_{\mathrm{FA}^*}(c)}{\int \rho_{\mathrm{FA}^*}(c)\mathrm{d}c} \tag{A20}$$

$$= \frac{\exp(-\beta\Delta\mu(c))P_{\mathrm{mf}}(c)}{\int \exp(-\beta\Delta\mu(c))P_{\mathrm{mf}}(c)\mathrm{d}c} \ . \tag{A21}$$

Here, from Eq. (A20) to Eq. (A21), we canceled λ because it appeared both in the numerator and denominator of the equations.

$P_{\mathrm{mf}}(c)$ denotes the density of Arp2/3 binding sites on F-actin at curvature c, relative to the total density of the binding sites:

$$P_{\mathrm{mf}}(c) := \frac{\rho_F^{\mathrm{total}}(c)}{N_{\mathrm{F}}} \tag{A22}$$

where the total binding site density N_{F} is independent of curvature. Thus, the relative branch density $\tilde{P}(c)$ is mathematically described by

$$\tilde{P}(c) := \frac{P(c)}{P_{\mathrm{mf}}(c)} \tag{A23}$$

$$= \frac{1}{\Pi}\exp(-\beta\Delta\mu(c)) \tag{A24}$$

where the normalization constant Π is

$$\Pi = \int \exp(-\beta\Delta\mu(c))P_{\mathrm{mf}}(c)\mathrm{d}c \ . \tag{A25}$$

Appendix B: On–rate of cofilin binding

A positive correlation between the on–rate of cofilin binding and fluctuation of F-actin was presented experimentally [24]. To elucidate this correlation based on our model, we expressed the on–rate, k_{on}, as a function of torsional fluctuation of F-actin based on our model. As shown in the experiment [24], the off-rate, k_{off}, was almost constant regardless of the fluctuation. Therefore, the dependence of the on–rate on the fluctuation can be derived from the dependence of the equilibrium constant, K_{e}, on the fluctuation (cf. $K_{\mathrm{e}} = k_{\mathrm{on}}/k_{\mathrm{off}}$). Because Hayakawa et al. analyzed the data in terms of the magnitude of fluctuation, we should be able to derive the equilibrium constant at a given magnitude of the fluctuation. Thus, the ensemble average of $K_{\mathrm{e}}(\theta)$ shall be taken with respect to torsional angle θ at constant κ (equivalently, constant magnitude of fluctuation) as follows.

$$K_{\mathrm{e}} = \int P_{\mathrm{f}}(\theta)\exp\left(-\beta\Delta\mu\left(\theta\right)\right)\mathrm{d}\theta \tag{B1}$$

$$P_{\mathrm{f}}\left(\theta\right) = \frac{1}{Z}\exp\left(-\beta\frac{\kappa\theta^2}{2\delta_0}\right) \tag{B2}$$

$$Z = \int \exp\left(-\beta\frac{\kappa\theta^2}{2\delta_0}\right)\mathrm{d}\theta \tag{B3}$$

Here, $P_{\mathrm{f}}(\theta)$ is the probability density of F-actin for torsion angle θ, which adopts the Boltzmann distribution, and Z is the partition function. Note that, if the chemical potential difference $\Delta\mu(\theta)$ is not dependent on the torsional angle θ, Eq. (B1) indicates that K_{e} can be a constant regardless of the torsional rigidity (equivalently, the torsional fluctuation). This is not the case with the experiment. Thus, we expect that the dependence of the on-rate on the fluctuation represents evidence for the dependence of $\Delta\mu(\theta)$ on θ.

Taking into account the rotational symmetry of the F-actin helix, integrations in Eqs. (B1) and (B3) are performed in the interval $[-\pi : \pi]$, and thus,

$$K_{\mathrm{e}} = 2\pi Z^{-1}\exp\left(-\beta\left(\Delta\mu(\theta_{\mathrm{i}}) + \frac{\kappa\theta_{\mathrm{i}}^2}{2\delta_0}\right)\right) \ . \tag{B4}$$

Upon calculation, we substitute Eq. (9) into $\Delta\mu(\theta)$ on the right hand side of Eq. (B1).

Because $\beta\kappa/\delta_0$ is of the order of 10^2, the exponential term in Eq. (B3) decreases steeply as $|\theta|$ increases. Thus, the integration interval can be changed to an infinite interval, and thus we can simply calculate the partition function,

$$Z = \sqrt{\frac{2\pi\delta_0}{\beta\kappa}} \ . \tag{B5}$$

Since Hayakawa et al. expressed the fluctuation by their originally defined parameter "index of fluctuation" (IF), we should normalize the torsional fluctuation to compare the model prediction with the experimental results. We choose an arbitrary reference state r, and then normalized the equilibrium constant K_{e} by its value at the reference state.

$$\frac{K_{\mathrm{e}}}{K_{\mathrm{e}}^{(\mathrm{r})}} = \sqrt{\frac{\kappa}{\kappa_{\mathrm{r}}}}\exp\left(-\beta\frac{\kappa_{\mathrm{r}}\theta_{\mathrm{i}}^2}{2\delta}\left(\frac{\kappa}{\kappa_{\mathrm{r}}} - 1\right)\right) \tag{B6}$$

$$= \sqrt{\frac{\langle\theta_{\mathrm{r}}^2\rangle}{\langle\theta^2\rangle}}\exp\left(-\beta\frac{\kappa_{\mathrm{r}}\theta_{\mathrm{i}}^2}{2\delta}\left(\frac{\langle\theta_{\mathrm{r}}^2\rangle}{\langle\theta^2\rangle} - 1\right)\right) \tag{B7}$$

From Eq. (B6) to Eq. (B7), we used the law of equipartition of energy, $\kappa\langle\theta^2\rangle = 1/\beta$. Finally, using the experimental evidence that k_{off} is almost constant regardless of the fluctuation, we obtain Eq. (17) as follows.

$$\frac{K_{\mathrm{e}}}{K_{\mathrm{e}}^{(\mathrm{r})}} = \frac{k_{\mathrm{on}}k_{\mathrm{off}}^{(\mathrm{r})}}{k_{\mathrm{on}}^{(\mathrm{r})}k_{\mathrm{off}}} \tag{B8}$$

$$= \frac{k_{\mathrm{on}}}{k_{\mathrm{on}}^{(\mathrm{r})}} \tag{B9}$$

[1] T. D. Pollard, and G. G. Borisy, Cell **112**, 453 (2003).
[2] R. Dominguez, and KC. Holmes, Annu. Rev. Biophys. **40**, 169 (2011).
[3] L. Blanchoin, R. Boujemaa-Paterski, C. Sykes, and J. Plastino, Physiol. Rev. **94**, 253 (2014).
[4] C. Revenu, R. Athman, S. Robine, and D. Douvard, Nat. Rev. Mol. Cell Biol. **5**, 635 (2004).
[5] S. J. Winder and K. R. Ayscough, J. Cell. Sci. **118**, 651 (2005).
[6] J. Baum, A. T. Papenfuss, B. Baum, T. P. Speed, and A. F. Cowman, Nat Rev Microbiol **4**, 621 (2006).
[7] B. Guo and W. H. Guilford, Proc. Natl. Acad. Sci. U. S. A. **103**, 9844 (2006).
[8] K. Hayakawa, H. Tatsumi, and M. Sokabe, J. Cell Biol. **195**, 721 (2011).
[9] T. QP. Uyeda, Y. Iwadate,N. Umeki, A. Nagasaki, and S. Yumura, PLoS ONE **6**, e26200 (2011).
[10] V. I. Risca, E. B. Wang, O. Chaudhuri, J. J. Chia, P. L. Geissler, and D. A. Fletcher, Proc. Natl. Acad. Sci. U. S. A. **109**, 2913 (2012).
[11] Y. V. Pereverzev, O. V. Prezhdo, M. Forero, E. V. Sokurenko, and W. E. Thomas, Biophys J. **89**, 1446 (2005).
[12] W. E. Thomas, V. Vogel, and E. Sokurenko, Annu. Rev. Biophys. **37**, 399 (2008).
[13] F. Reif, *Fundamentals of Statistical and Thermal Physics* (McGraw-Hill Int. Ed. 1985).
[14] C. C. Beltzner and T. D. Pollard, J. Biol. Chem. 283, 7135 (2008).
[15] B. A. Smith, K. Daugherty-Clarke, B. L. Goode, and J. Gelles, Proc. Natl. Acad. Sci. U. S. A. **110**, 1285 (2013).
[16] L. A. Helgeson, J. G. Prendergast, A. R. Wagner, M. Rodnick-Smith, and B. J. Nolen, J. Biol. Chem. 289, 28856 (2014).
[17] N. Volkmann, C. Page, R. Li, and D. Hanein, European Journal of Cell Biology 93, 179 (2014).
[18] A. D. White, A. J. Keefe, J. R. Ella-Menye, A. K. Nowinski , Q. Shao, J. Pfaendtner, and S. Jiang, J. Phys. Chem. B. **117**, 7254 (2013).
[19] C. P. Broedersz and F. C. MacKintosh, Rev. Mod. Phys. **86**, 995 (2014).
[20] J. Bamburg, A. McGough, and S. Ono, Trends Cell Biol. **9**, 364 (1999).
[21] H. Yamaoka and T. Adachi, Int. J. Mech. Sci.**52**, 329 (2010).
[22] S. Matsushita, Y. Inoue, M. Hojo, M. Sokabe and T. Adachi, J. Biomech **44**, 1776 (2011).
[23] B. R. McCullough, L. Blanchoin, J.-L. Martiel, and E. M. De la Cruz, J. Mol. Biol. 381, 550 (2008).
[24] K. Hayakawa, S. Sakakibara, M. Sokabe, and H. Tatsumi, PNAS **111**, 9810 (2014).
[25] H. Yoshimura, T. Nishio, K. Mihashi, K. Kinosita Jr., and A. Ikegami, J. Mol. Biol. **179**, 453 (1984).
[26] E. Muto, H. Sakai and K. Kaseda, J. Cell Biol. **168**, 691 (2005).
[27] H. Kojima,A. Ishimura and T. Yanagida, Proc. Natl. Acad. Sci. U. S. A. **91**, 12962 (1994).
[28] D. Y. Wong and D. Sept, J. Mol. Biol. **413**, 97 (2011).